FAILURE INVESTIGATION AND RETROFIT STRATEGIES OF A 22-SPAN STEEL GIRDER BRIDGE DURING THE 2010 CHILE EARTHQUAKE

Zuocai Wang[1], Genda Chen[2], Phillip W. Yen[3], and Ian Buckle[4]

Abstract

This paper presents a case study on the Cardinal Raúl Silva Henŕiquez Bridge that was significantly damaged during the Chile Earthquake on February 27, 2010. Field observations and finite element simulations indicated that the bridge failed mainly because the excessive longitudinal load of 22 continuous steel-girder spans was transferred from the girders to their bearing masonry plates at two abutments with a weld connection detail, locally bending the girders due to axial load eccentricity. Parametric studies demonstrated that an effective retrofit strategy can be developed by reducing the number of continuous spans, modifying the connection detail, and increasing the capacity of girders with enlarged bearing seats, additional stiffeners for girders, and thicker flanges and webs.

Introduction

On February 27, 2010, the M8.8 offshore Maule earthquake occurred on a thrust fault along the boundary between the Nazca and South American tectonic plates [USGS, 2010]. The Chile earthquake damaged about 200 bridges and led to 20 collapses. One of the significantly damaged bridges is the Cardinal Raúl Silva Henŕiquez Bridge. Based on the field inspections by Chen et al. [2010], bottom flanges and webs of the steel girders at abutment supports and the girder-to-abutment weld connections were severely fractured during the earthquake. This type of damage is indicative of the presence of excessive longitudinal loads in the bridge superstructure since only one center expansion joint exists in the entire bridge structure. In addition, the bottom flanges of the girders were welded on masonry steel plates at abutments. This detail is not representative to the common practice in continuous steel girder bridge constructions where a continuous bridge section is simply supported on one fixed bearing and multiple expansion bearings [Saadeghvaziri et al., 2000]. The specific girder-to-abutment connection detail in the Cardinal Raúl Silva Henŕiquez Bridge attracted not only axial and shear forces but also a bending moment in the longitudinal plane of the bridge under earthquake loads.

---

[1] Ph.D. Candidate, Dept. of Civil, Architectural, and Environmental Engineering, Missouri University of Science and Technology, Rolla, MO, USA
[2] Professor, Dept. of Civil, Architectural, and Environmental Engineering, Missouri University of Science and Technology, Rolla, MO, USA
[3] Research Structural Engineer, Turner Fairbank Highway Research Center, Federal Highway Administration, McLean, VA, USA
[4] Dept. of Civil and Environmental Engineering, University of Nevada, Reno, NV, USA

Previous research concluded that steel bridge superstructures are susceptible to damage under low or moderated earthquakes and even more fragile than concrete superstructures if designed improperly [Itani et al., 2004]. For example, bearing failure in the steel girder bridges that were designed without seismic considerations has been commonly seen during previous earthquake events due to insufficient seat length. The load path and the capacity of a bridge system and its individual components at end supports must be evaluated case by case.

The objectives of this study are to investigate the failure mechanism of girders and end bearings at two abutments of the Cardinal Raúl Silva Henŕiquez Bridge during the 2010 Chile Earthquake and develop various effective retrofit strategies for them through sensitive studies with a finite element model of the bridge.

Bridge Description and Field Observed Damage

(1) Configuration of the Bridge

Built in 2002, Cardenal Raúl Silva Henŕiquez Bridge is a 22-span, steel-girder structure crossing the Maule River near Constitución in the NE-SW direction. Each span length is 41.5 m. The bridge is supported by two seat-type abutments and twenty-one intermediate bents. As partially shown in Fig. 1, the first five bents from the NE abutment are supported on two reinforced concrete (RC) columns and drilled shafts. The next six bents are supported on three RC columns and drilled shafts. The following eight bents are steel pile bents with three legs (one vertical and two inclined) with horizontal struts and diagonal braces interconnecting the legs in each bent. The last two bents are supported on three RC columns that rest on footings. The bridge superstructure is comprised of two continuous 11-span-long segments with three expansion joints at the two ends and in the middle of the bridge. It is connected to the bridge substructure by elastomeric pads at all piers to allow for longitudinal movement except for two abutments. At each abutment, three girders were welded to their bearing masonry plates that are anchored into the abutment.

Fig. 1 Cardenal Raúl Silva Henŕiquez Bridge

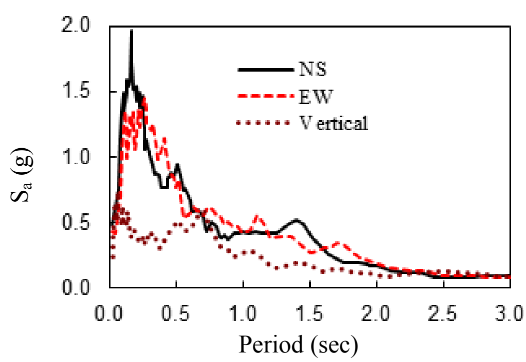

Fig. 2 Acceleration Response Spectra

(2) Acceleration Response Spectra

The 2010 Chile earthquake generated ground motions with long duration and multiple pulses [Boroschek et al., 2010]. The three-component earthquake ground motions at the Hospital Station in Curicó near the bridge site were successfully recorded but not released to the public as of today. However, their acceleration response spectra were made available as shown in Fig. 2. It can be seen from Fig. 2 that the NS and EW acceleration spectra are much larger than the vertical acceleration spectrum in a period range from 0.2 sec to 0.6 sec and from 0.8 sec to 1.5 sec. On the other hand, the natural periods of the particular steel-girder bridge almost fall in this range. In other words, the bridge is more sensitive to the longitudinal and transverse motions.

(3) Field Observed Damage

During the earthquake, the NE portion of the bridge moved transversely from west to east as shown in Fig. 3(a). All steel stoppers were deformed and girders were displaced from their elastomeric pads, resulting in the web and flange bending of the exterior girder about its weak axis. At the NE abutment, the webs and bottom flanges were fractured in all three girders, and both bearing stiffener and web buckled as illustrated in Fig. 3(b). The cause of this type of damage is indicative of excessive longitudinal loads in the superstructure that was resisted by the weld bearing connection at the abutment. At the SW abutment, the welds from the girder bottom flanges to the masonry plates were fractured [Chen et al., 2010].

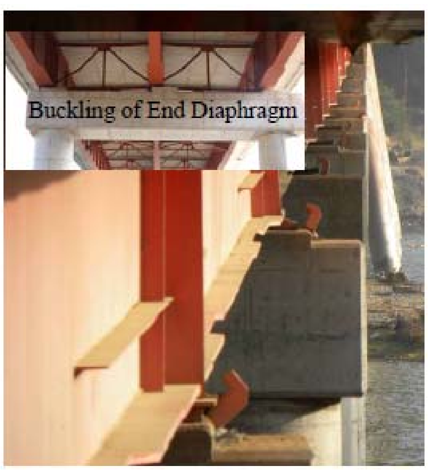

(a) Girder offset and cross frame buckling (b) Girder fracture at the north abutment

Fig. 3 Superstructure Damage at the NE Portion

Response Spectrum Analysis of the Bridge System

(1) The Grillage Finite Element Model

A typical cross section of the bridge is schematically shown in Fig. 4. The bridge has a total of 12 types of cross sections with various flange widths and thicknesses. The flange width of steel girders varies from 0.25 m to 0.62 m, and the thickness changes from 12 mm to 40 mm. The height and thickness of girder webs are 2.06 m and 12 mm, respectively. The bridge has two types of steel diaphragms spaced every 2 m. It also has two types of piers: concrete and steel pile bents. The diameter of circular concrete columns is 1.5 m while the outer diameter of the 12-mm thick thin walled circular steel pile is 1.0 m. The concrete bridge deck is 10 m wide and its thickness is 0.25 m.

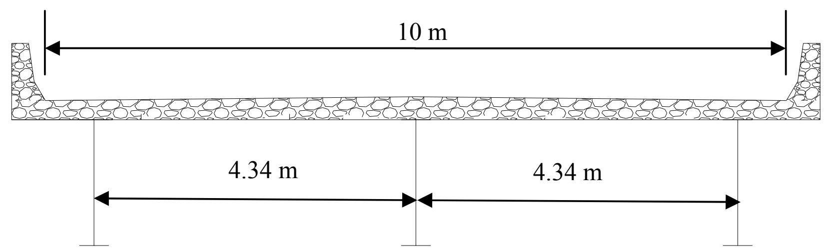

Fig. 4 Bridge Cross Section

To understand its complicated seismic behavior, a grillage mesh finite element model was established to represent the global responses of the entire bridge, and a detailed three-dimensional (3-D) model was created for the local failure analysis of the fractured girder portion. In the global grillage model as shown in Fig. 5, the beam elements were used to represent the bridge decks and other components (girders, bent caps, and columns). The longitudinal beam elements represent the centerline of bridge members passing through the neutral axis of all cross sections. The moment of inertia, cross sectional area and unit mass of the longitudinal grillage members were determined from the properties of as-built girders and a portion of bridge decks based on the effective width of composite beams [Eugene and Damien, 2005].

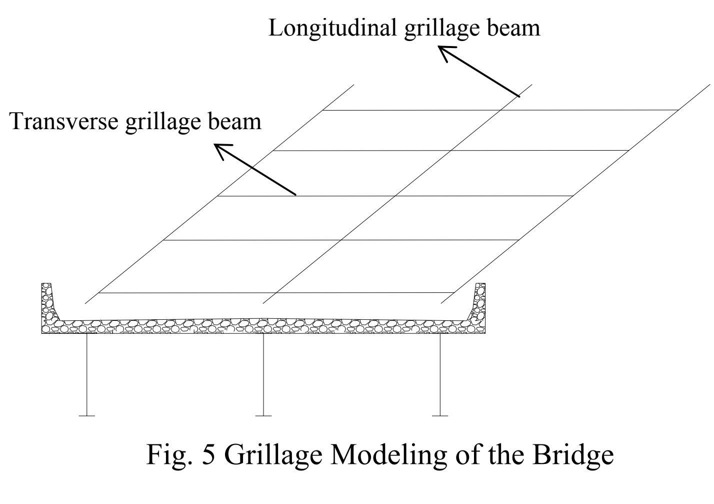

Fig. 5 Grillage Modeling of the Bridge

All transverse grillage members were placed at the location of diaphragms. Their properties were directly calculated from the as-built diaphragm frames. The equivalent cross area and moment of inertia of each diaphragm frame were calculated based on the equivalent displacement criterion. The properties of bent caps and columns (reinforced concrete or steel tube) were estimated based on their as-built cross sections. The cross sectional areas and moments of inertia of various grillage members are presented in Table 1. Here, I_x and I_y represent the moments of inertial about the strong (horizontal) and weak (vertical) axes of a cross section, respectively. The Young's Modulus of Elasticity for the longitudinal and transverse grillage beams and steel tubes is 2×10^{11} N/m^2, while that for the concrete bent caps and columns is 2.5×10^{10} N/m^2.

Table 1 Section Properties of Grillage Beam Elements

Grillage beams		Area (m^2)	I_x (10^{-3} m^4)	I_y (10^{-3} m^4)
Longitudinal	1	0.17	51.4	3.3
	2	0.18	92	3.5
	3	0.19	107	3.7
	4	0.19	119	3.9
	5	0.19	123	4
	6	0.18	99	3.5
	7	0.17	84	3.4
	8	0.19	116	3.8
	9	0.21	159	4.4
	10	0.17	78	3.4
	11	0.19	130	4.2
	12	0.18	98	3.5
Transverse	1	0.003	0.002	0.0002
	2	0.007	4.67	0.001
Concrete column		1.78	249	249
Steel pipe		0.04	4.55	4.55

To take into account soil-foundation-structure interaction, all columns in each bent were simply considered to be fixed at certain depth that can be estimated by [Davisson and Robinson, 1965]:

$$L_f = 1.8\left[\frac{EI}{n_h}\right]^{0.2} \tag{1}$$

in which E and I are the modulus of elasticity and the moment of inertia of columns, respectively, and n_h is the coefficient of the horizontal subgrade modulus of soil materials. The grillage finite element model of the entire bridge was set up with SAP2000 as shown in Fig. 6.

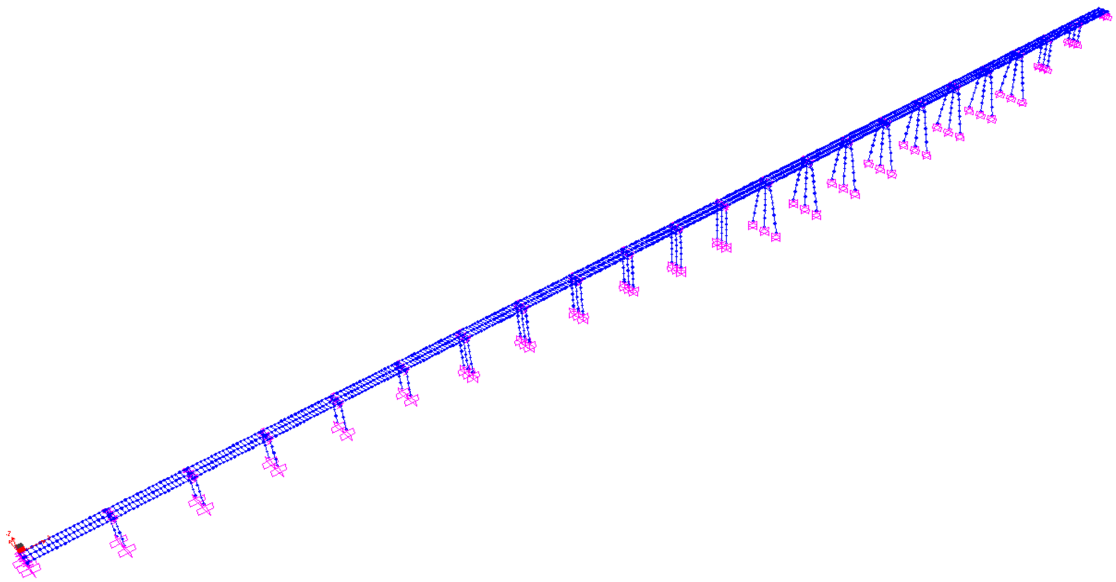

Fig. 6 Finite Element Model of the Bridge based on Grillage Method

(2) Response Spectrum Analysis

The complete quadratic combination (CQC) rule was applied to combine the effects of modal responses [Chopra, 2007]. Therefore, the peak value of a structural response can be written as:

$$r_o = \left(\sum_{i=1}^{N}\sum_{n=1}^{N} \rho_{in} r_{io} r_{no}\right)^{1/2} \tag{2}$$

where N represents the total number of vibration mode of engineering interest; r_0 is a peak response of the bridge system; r_{io} and r_{no} are the peak responses of the ith and nth modes of vibration, respectively; and ρ_{in} is the correlation coefficient between the two modes.

The natural frequencies of the first transverse, first vertical, and first torsional modes of vibration are listed in Table 2. The maximum axial force, bending moment, and shear of the NE end girders where significant damage was observed are presented in Table 3. It can be seen from Table 3 that the maximum axial force is 8750 kN mainly due to the longitudinal earthquake ground motion. Due to load transfer eccentricity (2 m) at each end of the bridge, the axial force causes a significant bending moment at the end of each girder, which is most likely underestimated in design. This moment is almost 6 times as large as that of the bending moment directly caused by the earthquake load.

Table 2 Natural Frequencies of the First Transverse, Longitudinal, Vertical and Torsional Modes

1st Mode	Transverse	Longitudinal	Vertical	Torsional
Natural frequency (Hz)	0.45	1.21	1.85	2.05

Table 3 Maximum Axial Force, Bending Moment, and Shear at the NE End Girders

Axial force (kN)	Moment (kN-m)	Shear (kN)
8750	2970	240

3D Finite Element Model for the Fracture Analysis of Girders

To better understand the stress concentration around the fracture location of girders, the area of crack initiation, and the process of failure, a 3D finite element model of a small portion of girder (including bearing stiffeners) was established with ABAQUS. Considering 0.7 m fillet weld on the bottom flange of each girder at the abutments or 0.7 m bearing seat length, the detailed 3D model is selected to be 1.7 m long as schematically illustrated in Fig. 7(a). The steel girder and reinforced concrete deck were modeled by plate and solid elements, respectively, as shown in Fig. 7(b). The portion of the bottom flange of the girder, welded on the masonry plate at abutments, was fixed in the fracture analysis of girders. The flange width and thickness of the girder are 0.28 m and 12 mm, respectively. The web and stiffener thicknesses are 12 mm and 20 mm, respectively. The maximum axial force obtained at the end of girders from the global grillage model of the bridge system was divided into two components based on the weight ratio between the bridge deck and steel girders. Each component was uniformly distributed and applied on its respective deck or girder cross section.

To understand the crack initiation and failure process, four (4) load cases were considered for elastic-plastic analysis: 130, 300, 440, and 700 kN. The stress distribution for each case is presented in Fig. 8. It can be observed from Fig. 8 that damage likely initiated at the bottom flange of the girder under an axial load of 130 kN. Cases 2 and 3 in Fig. 8 indicate that the maximum stress will extend into the girder web in the area of observed damage after the Chili Earthquake. Eventually, the girder failed at an axial force of 700 kN, which is 8% of the maximum axial load obtained from the response spectrum analysis. Based on the stress distributions under various load cases and field observations, it was verified that the web fracture was indeed caused by the excessive longitudinal load, which can be estimated to be approximately 12 times of the actual capacity of the steel girder bearing system.

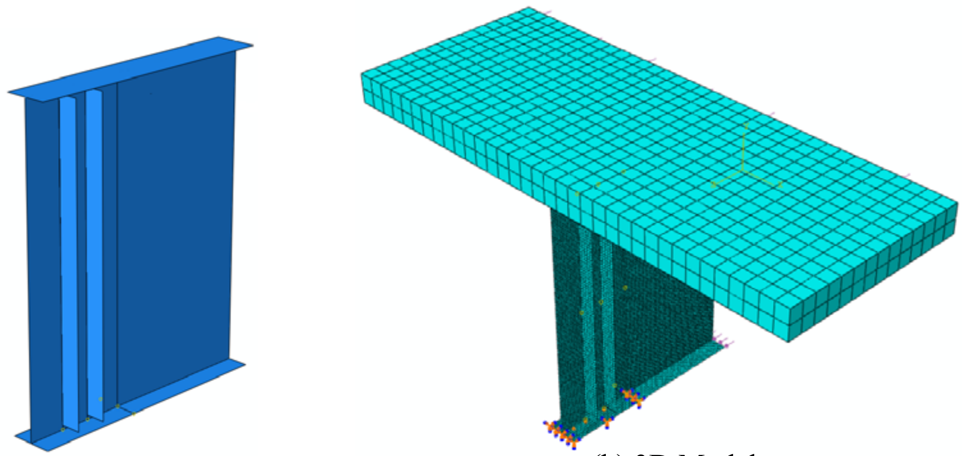

(a) Steel Girder (b) 3D Model

Fig. 7 Modeled Portion of Steel Girder and ABAQUS 3D Finite Element Model

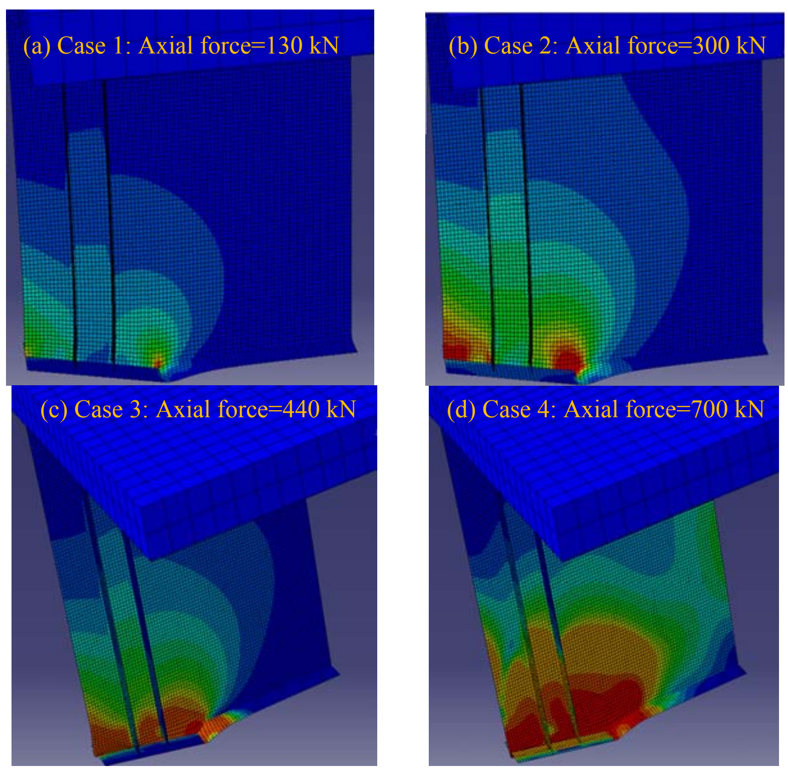

Fig. 8 Stress Distribution under Each of Four Axial Forces

Parametric Study

In this section, several potential retrofit strategies are investigated either by reducing the longitudinal earthquake load or increasing the seismic capacity to ensure a smooth transfer of the seismic load from the girder to abutment. To limit the scope of work, it is assumed that both abutments are adequate to transfer the seismic loads from the bridge superstructure to ground. Example retrofit strategies for the bearing connections include:

1. Reducing the longitudinal seismic load by increasing the number of joints in bridge superstructure (both deck and girder) so that bearing elements between the super- and sub-structure can transfer the seismic load satisfactorily,
2. Changing the bearing connection detail between the bottom flange of girders and the masonry plate of abutments, and
3. Increasing the seismic capacity of the girder-to-abutment system by increasing the thicknesses of web and bottom flange, the number of stiffeners, and the bearing area at abutments.

More advanced retrofit strategies include the use of base isolators at each bent and abutment so that the longitudinal load on each bent can be regulated based on its available capacity for load transfer, and the use of passive energy dissipation systems so that earthquake energy can be dissipated. In what follows, only the three strategies that are detailed above are discussed.

(1) Number of Joints

One effective way to reduce the longitudinal seismic force is to increase the number of joints at intermediate bents. Towards this endeavor, the number of continuous spans was considered to be 1, 2, 3, 4, 5, and 6. In each case, the longitudinal force calculated from the response spectrum analysis based on the grillage beam model is shown in Fig. 9. It can be clearly seen from Fig. 9 that the axial force is significantly reduced as the number of continuous spans is reduced.

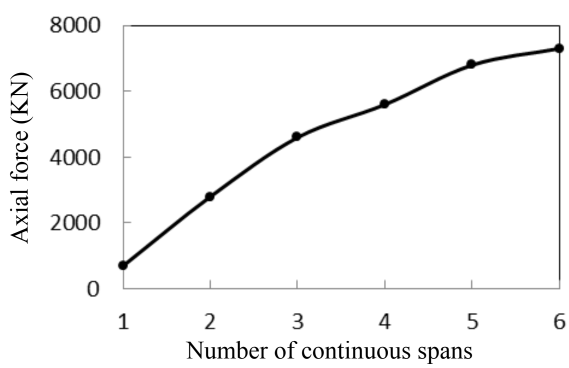

Fig. 9 Axial Force at the End Girder of Bridge with Various Continuous Span Numbers

On the other hand, more expansion joints in bridge deck mean more maintenance since these are often the areas for water leakage and corrosion developed over the years. Furthermore, as the number of expansion joints increases, the redundant effects for extreme loads diminish. Therefore, there must be a tradeoff between seismic performance and maintenance cost in practical applications or advanced retrofitting strategies with dampers and isolators can be developed.

(2) Bearing Connection Detail

Bearing capacity can be increased by using thicker web and bottom flange of girders, additional stiffeners, and extended bearing seat. For parametric studies, a total of 18 elastic-plastic analyses of the 3D finite element model of girders were conducted with complete combinations of the following parameters:

1. Thickness of web and bottom flange = 12, 25, and 50 mm,
2. Bearing seat length = 0.7. 1.0, and 1.2 m, and
3. Additional web stiffener of 30 mm thick = 0 and 3 as illustrated in Fig. 10.

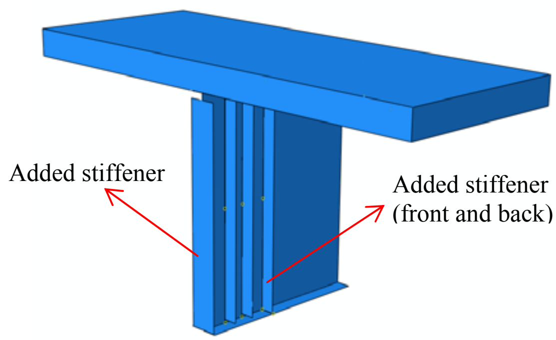

Fig. 10 Three Added Stiffeners at the End of the Girder

The additional stiffeners were considered to be welded on the web and the bottom flange of the girder. They function as tension and compression members under the end bending moment caused by the longitudinal earthquake load and help transfer them from the girder to the masonry plate and then abutment.

The axial force capacities of the retrofitted bearing connection at the end of the girder are listed in Table 4 with no added stiffeners and in Table 5 with three added stiffeners. The axial force is considered to be applied at the same location as the seismic axial load determined from the global bridge analysis.

Table 4 Axial Load Capacities of Retrofitted Bearing Connections with no Added Stiffeners (kN)

Plate thickness (mm)	Bearing seat length (m)		
	0.7	1	1.2
12	710	1226	1612
25	1568	2575	3425
50	3180	5309	6982

Table 5 Axial Force Capacities of Retrofitted Bearing Connections with Three Added Stiffeners (kN)

Plate thickness (mm)	Bearing seat length (m)		
	0.7	1	1.2
12	2137	3215	3907
25	2961	4599	5843
50	4520	7192	9329

In retrofitted design, the seismic capacity of the structure must be larger than the seismic demand by a certain safety margin. As indicated in Tables 4 and 5 for the Cardenal Raúl Silva Henŕiquez Bridge, only when the thickness of the web and flange is increased to 50 mm, three 30 mm thick stiffeners are added at the girder end, and the bearing seat is lengthened to 1.2 m can the retrofitted bearing connection transfer the excessive longitudinal earthquake load from the girder to abutment without requiring additional expansion joints over intermediate bents. If the number of continuous spans is reduced, the longitudinal earthquake load can be significantly reduced and thus more bearing connection retrofitting options in Tables 4 and 5 are viable in design. For instance, Fig. 11 shows the seismic demand versus seismic capacity for various combinations of reducing span numbers and increasing web/flange thickness and bearing seat length; when the bridge girders are simply supported, the current bridge design can transfer the earthquake-induced load. For a specified continuous span number, the seismic demand (axial load) can be determined from a global bridge analysis as shown in dash line in Fig. 11. Various retrofitting options as shown in solid, dotted, and long dash dotted lines in Fig. 11, which can increase the seismic capacity (axial force) above the seismic demand, can be considered as viable designs with adequate performance.

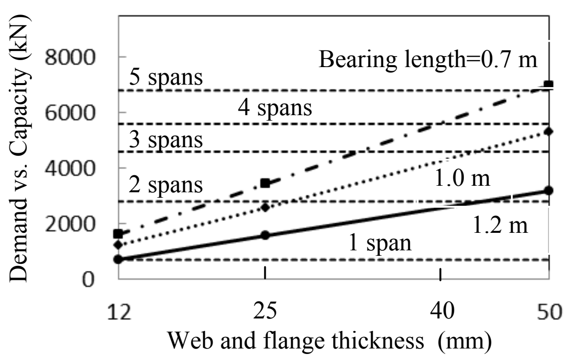

(a) With no Added Stiffener

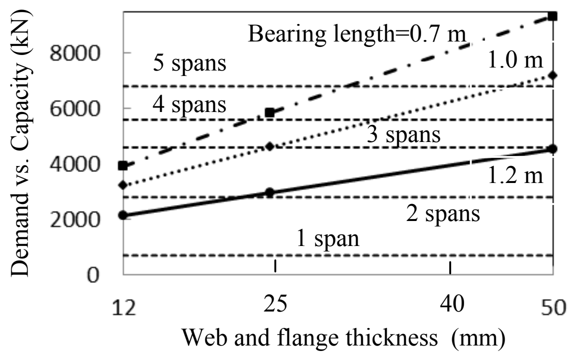

(b) With Three Added Stiffeners

Fig. 11 Seismic Demand (Load) versus Seismic Capacity (Force) for Various Continuous Span Numbers and Bearing Connection Retrofit Designs

Fig. 11 also indicates that if the bearing weld connection were changed to a pin connection, the bending moment due to the welded bottom flanges of girders at abutments would disappear and the bending moment due to load eccentricity would be approximately 8750-2970 = 5780 kN. Indeed, re-running the grillage beam model with pin supports at two abutments gave a moment of 6800 kN. Even with pin supports, the bridge must be retrofitted further by increasing seismic capability such as adding three stiffeners and/or increasing web/flange thicknesses. The main difference between the pin and fixed supports, however, lies in the design of masonry plates and abutments. With pin supports, the masonry plates are subjected to both axial and shear forces only, which can be significantly less demanding in comparison with the fixed supports as seen in the current bridge design.

Conclusions

To understand the main causes of the steel girder fracture and weld fracture of a 22-span Cardenal Raúl Silva Henŕiquez Bridge during the 2010 Chile Earthquake, a grillage beam model of the entire bridge system and a 3D finite element model of the bearing connection at bridge abutments have been developed. The representative acceleration response spectra at the Hospital Station in Curicó near the bridge site were used for the global bridge analysis. Parametric studies were conducted to investigate the effects of various retrofit designs at bearing connections. Following is a summary of the preliminary findings from this study:

1. The current bridge design has 11 continuous spans that are all rested on elastomeric bearings except for end bearing connections at abutments. The elastomeric bearings allow for some longitudinal displacement under the longitudinal component of ground motions. Therefore, the fixed girder-to-abutment bearing connection attracted the longitudinal load of all continuous spans, causing fracture damage at abutments.
2. Reducing the number of continuous spans can significantly reduce the longitudinal load applied at the bearing connection system. However, the

current bearing connection design is still inadequate to transfer the longitudinal load unless all girders are simply supported. Their combinations may be necessary to transfer the loads induced by a mega earthquake such as the 2010 M8.8 Chile Earthquake.

3. Increasing the web and flange thickness of girders, number of stiffeners, and length of bearing seats at the bearing connection are all effective measures for seismic retrofitting of the bridge.
4. For the multi-span bridge structure, the longitudinal component of the 2010 Chile Earthquake induced ground motions caused more significant damage than the vertical earthquake motion. Therefore, due considerations must be taken of the longitudinal ground motion effect in bridge design and a decision may have to be made to trade off the seismic design load and the seismic redundancy in lieu of the number of continuous spans.

References

USGS, Magnitude 8.8 – Offshore Maule, Chile, February 27, 2010, http://earthquake.usgs.gove/earthquakes/eqinthenews/2010/us2010tfan/, Earthquake Hazards Program, 2010.

Chen, G.D., Yen, P. W., Buckle, I., Allen, T., Alzamora, D., Ger, J., and Arias, J. G.: 2010 Chile Earthquake Implications to the Seismic Design of Bridges, Proceedings of the 26th US-Japan Bridge Engineering Workshop, pp. 203-216, 2010.

Saadeghvaziri, M. A., Yazdani-Motlagh, A. R., and Rashidi, S.: Effects of Soil-Structure Interaction on Longitudinal Seismic Response of MSSS Bridges, Soil Dynamics and Earthquake Engineering, vol. 20, No. 1-4, pp. 231-242, 2000.

Itani, A. M., Bruneau, M., Carden, L., and Buckle, I. G.: Seismic Behavior of Steel Girder Bridge Superstructures, Journal of Bridge Engineering, Vol. 9, No. 3, pp. 243-249, 2004.

Boroschek, r., Soto, P., Leon, R., and Comte, D.: Terremoto Centro Sur Chile-27 de Febrero de 2010, Informe Preliminar Nº 4, Unversidad de Chile-Depto. Ingenierial Civil, and Depto. De Geofisica, 2010, 29pp.

Eugene J. and Damien L. K.: Bridge Deck Analysis, Taylor & Francis e-Library, 2005, 278pp.

Davisson, M. T., and Robinson, K. E.: Bending and Buckling of Partially Embedded Piles, Proceedings of 6th International Conference on Soil Mechanics and Foundation Engineering, Canada, Vol. III, pp. 243-246, 1965.

Chopra, A. K.: Dynamics of Structures-Theory and Application to Earthquake Engineering, Prentice-Hall, Inc., New Jersey, U.S.A., 2007, 876pp.